Minute-timescale simulations of G Protein Coupled Receptor A2A activation mechanism reveals a receptor pseudo-active state

*Vincenzo Maria D'Amore,[1] Paolo Conflitti,[2] Luciana Marinelli,[1] Vittorio Limongelli [2]**

[1]Dipartimento di Farmacia, Università degli Studi di Napoli "Federico II", Via D. Montesano 49, 80131 Naples, Italy.

[2]Faculty of Biomedical Sciences, Euler Institute, Università della Svizzera italiana (USI), via G. Buffi 13, CH-6900 Lugano, Switzerland.

*Corresponding author. Email: vittoriolimongelli@gmail.com

ABSTRACT

G protein-coupled receptors (GPCRs) are a most prominent pharmacological target, regulating various biological functions and targeted by over one third of marketed drugs. These receptors are activated by orthosteric ligands and undergo large conformational changes that lead to coupling effector proteins. Despite their relevance, many aspects of their activation mechanism remain unclear, hampering rational drug design studies. In this work, we elucidate the activation mechanism of the adenosine A2A receptor (A2AR), a class A GPCR, using molecular dynamics simulations and free energy calculations. We have explored the entire conformational landscape of A2AR in its basal apo form and in differently ligated conditions, identifying the receptor's lowest energy functional states. Among these is a novel pseudo-active state (pAS) stabilised by specific "microswitch" residues interactions like the $R^{5.66}/E^{6.30}$ salt bridge. In this form, A2A is able to couple β-arrestin over G proteins, enlightening possible routes for biased signalling. Our findings shed light on GPCR activation dynamics, paving the way to the rational design of drugs for various diseases involving A2AR, including cancer, inflammation, cardiovascular, Parkinson's, and Alzheimer's diseases.

Introduction

G protein coupled receptors (GPCRs) are prominent pharmacological targets, representing 4% of the protein-coding genome and being targeted by almost 40% of the currently marketed drugs.[1,2] In response to extracellular stimuli like hormones, neurotransmitters, and odorants, GPCRs regulate a plethora of biological functions, including vision, inflammation, and sensory perception.[1] They show a conserved structural architecture arranged in seven transmembrane (TM) helices, connected through 3 extracellular (ECL) and 3 intracellular (ICL) loops.[3] The GPCR barrel-like tertiary structure can be depicted in three main sections (Fig. 1): i) the orthosteric ligand binding site (OBS) at the extracellular region; ii) the connector; and iii) the intracellular binding site (IBS) where binding of effector proteins (aka transducers) occurr.[4] The operating system is a ternary complex where GPCR is bound to a ligand and at the same time to a transducer that triggers the signal cascade inside the cell.[5] During its action, GPCR undergoes large-scale conformational changes passing from the inactive to the active state. For instance, in Rhodopsin-family class A GPCRs, the two terminal states - i.e., *active* and *inactive* - diverge for an outward/inward motion of the cytoplasmic end of TM6 (~ 12-14 Å), accompanied by a rotation of the same helix around its axis (~ 40°-50°) and slight shifts of the C-ter side of TM5 and TM7 (Fig. 1).[5–7] In doing so, the GPCR IBS opens up, promoting the

interaction with the transducer. On the other hand, minor differences (in the range of 1.5-2 Å) are detected comparing active and inactive structures at the OBS level.[8,9] Nonetheless, the receptor (de)activation appears to be regulated by a fine-grained allosteric communication between the two regions. Indeed, the binding of an agonist to OBS promotes the recruitment of an intracellular transducer at IBS; at the same time, the binary transducer-GPCR complex has higher affinity for agonist then the sole receptor.[10–12] In addition, GPCRs can trigger a wide range of cellular pathways[10,13,14,15] by coupling with diverse effector proteins such as G proteins (GPs)[13,15], G protein-coupled receptor kinases (GRKs)[16], proto-oncogene c-Src[17] and β arrestins[18,19]. In this scenario, a ligand might induce specific receptor conformations competent for the binding to a certain effector, thus selectively activating downstream cell signaling.[20–25] This phenomenon, known as "biased signalling"[20,22], brought to the fore new important implications for the pharmaceutical and clinical application of GPCR-targeting drugs.[20,23,26] For instance, developing molecules capable of selectively activating or inhibiting a specific signalling cascade can yield a more targeted modulation of cell function with consequently reduced adverse effects,[27,28] as recently reported for antidepressant drugs targeting the serotonin 5-HT_{2A} receptor,[29] and analgesics targeting adenosine A1[30] and μ opioid receptor[31]. Nevertheless, the rational design of "biased" ligands is hampered by the lack of structural information on all the functional conformations assumed by the GPCRs along their activation process. In fact, although the so-called "Resolution Revolution"[32] in structural biology is constantly advancing the molecular understanding of the terminal states, other fundamental aspects of the GPCRs' functional mechanism remain elusive, including the activation dynamics and the possible presence of receptor metastable, intermediate states. Atomistic simulations based on molecular dynamics (MD) techniques[9,33,42–49,34–41] have demonstrated ability in detecting dynamic properties of the receptor, including the interaction with ligands and effectors.[9,31,41–50,33–40]. However, the long - ms - timescale and the complex allosteric network ruling GPCR activation make it elusive even to sophisticated simulation protocols.

In the present work, we elucidate the activation mechanism of the adenosine A2A receptor (A2AR), a class A GPCR, providing structural and energetics information on all the functional conformations assumed by the receptor in different ligated conditions. In particular, we performed extensive MD simulations and enhanced sampling calculations that allowed disclosing the free energy landscapes of the (de)activation process of A2AR i) in the *apo* form; ii) in complex with the full agonist 5'-N-ethylcarboxamidoadenosine (NECA); and iii) in complex with the antagonist ZM241385 (ZMA). In each system, we have identified at atomistic resolution the lowest energy - hence most probable - states assumed by A2AR, rationalising the diverse pharmacological activity of the two investigated ligands. In particular, we elucidate the way they change the conformational free-energy landscape of the receptor passing from the active to the inactive form. Importantly, we disclose two structures of A2AR in the *apo* form that were not previously resolved and well explain the NMR and fluorescence data reported for this receptor.[11,51–56] One is similar to the inactive state experimentally found in presence of antagonist ligands. The other corresponds to a novel receptor conformation that we named *pseudo-active state* (pAS). This structure is characterized by a distinctive arrangement of the connector region and in particular TM6, with a state-specific orientation of the "activation microswitches" amino acids, such as $W^{6.48}$ (Ballesteros-Weinstein numbering used)[57] ("toggle switch"), the $E^{6.30}$/$DRY^{3.49-51}$, the $P^{5.40}I^{3.40}F^{6.44}$ and the $NPxxY^{7.49-53}$ motifs (Fig. 1).[36,58–61] Among these, the class A conserved residue $E^{6.30}$ plays a leading role during A2A dynamics, determining the TM6 rotation necessary for receptor activation. In particular, $E^{6.30}$ works as the key "activation" switch by interacting with $R^{3.50}$ in the A2A inactive state - forming the characteristic "inactivating ionic lock" (IIL) found in many GPCRs[58,59] - while in the active state it engages a salt bridge with $R^{5.66}$. The high phylogenetic conservation of $R^{5.66}$ in class A GPCRs makes the $E^{6.30}$/$R^{5.66}$ interaction a hallmark of receptor activation that we name

"activating ionic lock (AIL)". Interestingly, A2A in the newly identified pAS shows a higher affinity for β arrestin than G protein that merits to be further investigated in GPCRs biased signalling studies.

Our study reveals unprecedented structural insight into A2A activation mechanism that enhances our understanding of GPCRs functioning and might impact the rational design of biased ligands for this pharmacologically relevant target involved in several diseases including cancer, inflammatory, cardiovascular, Parkinson's and Alzheimer's diseases.[62–67]

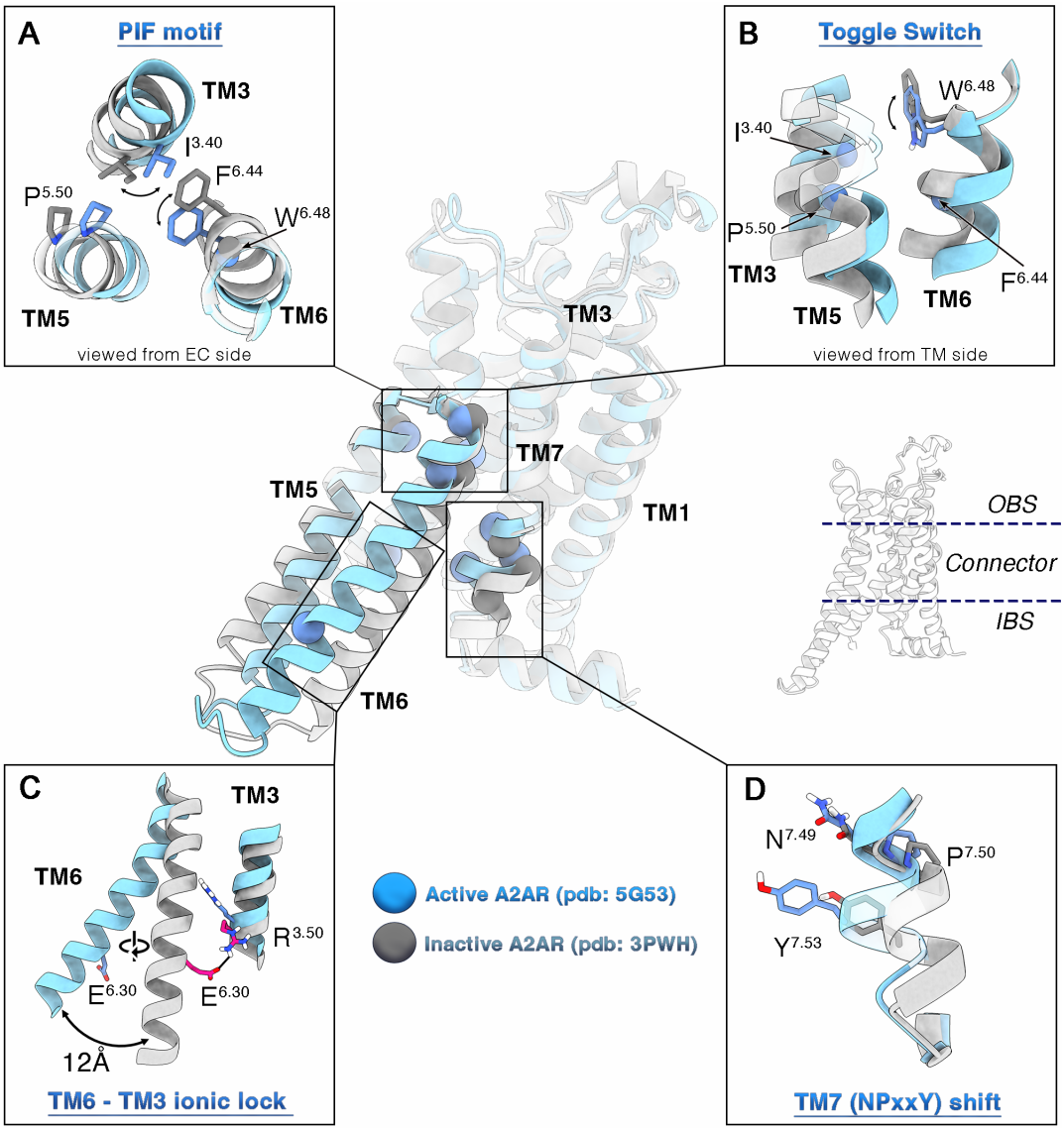

Figure 1. Main conformational changes occurring during GPCR activation. Active and inactive conformations of the A2AR are shown as light blue and silver cartoon, respectively. The four fundamental class A microswitches are highlighted as insets: the PIF motif (connector region, A), the W6.48 rotameric state "toggle switch" (OBS-connector region, B), the TM6-TM3 inactivating ionic lock ("IIL", IBS region, C) and the NPxxY inward/outward shift (IBS region, D). The residues mainly involved in these transitions are shown as spheres (representing the α-carbon) onto the central representations of active and inactive receptors, and as sticks in the insets. Non-polar hydrogens are omitted for sake of clarity.

Results

Effect of ligand binding and G protein recruitment on A2AR conformational dynamics

The A2A receptor can assume a large number of conformations ranging between an *active* state,[68,69] bound to agonist and G protein, and an *inactive* state,[60,70] typically induced by inverse agonist binding. In order to investigate how the diverse ligands and G protein influence the receptor dynamics, we first performed a series of extensive all-atom molecular dynamics simulations on differently ligated forms of A2AR. In particular, starting from the experimental structures of the *active* and *inactive* A2AR, we prepared seven distinct simulation systems in which the GPCR is coupled with pharmacologically diverse ligands - the agonist NECA, the antagonist/inverse agonist ZMA (its pharmacological profile is debated, e.g., see refs[85–87]) - and the miniGs heterotrimer (Gs) in all possible combinations (Table 1). The A2AR was embedded in a mixed POPC-cholesterol (7:3 ratio) membrane environment, and each system was simulated in explicit solvent for 5 μs, resulting in a total simulation time of approximately 35 μs.

Table 1. Summary of the simulated systems

Code Name	Starting Conformation	Ligand	G Protein coupling
FANG	Active	NECA (agonist)	Yes
FApoG	Active	None (*apo form)*	Yes
FAN	Active	NECA (agonist)	No
FApo	Active	None (*apo form)*	No
INeca	Inactive	NECA (agonist)	No
INapo	Inactive	None (*apo form)*	No
INzma	Inactive	ZMA (antagonist)	No

Our simulations allowed elucidating the stabilizing effect of orthosteric ligands and G protein on their binding sites, the OBS and the IBS, respectively. In the OBS, higher RMSD fluctuations are generally observed for the *apo* systems (*FApo, FApoG,* and *INapo*) compared to the *holo* ones (*FAN, FANG,* and *INzma*) (Supplementary Fig. S1). This phenomenon can be ascribed to the drug-protein interactions engaged by NECA and ZMA, which stabilize the OBS side chains conformations and consequently reduce the backbone fluctuation. Only the *holo Gs-uncoupled* system *INeca* shows relatively high RMSD values of the OBS. This is likely due to induced fit effects of the agonist NECA on the inactive form of A2A, which is not the natural host conformation of the receptor for this ligand. In fact, as no experimental structure of inactive A2A in complex with the agonist NECA is available, the starting state of the *INeca* simulation was obtained from docking the agonist into the *inactive* experimental structure of A2A (see Methods for details). The purpose of this simulation is to investigate how the ligand influences the receptor conformational dynamics starting from the inactive state and if it could drive the receptor towards the active state in absence of G protein.

Similarly to the ligands at OBS, Gs stabilises the IBS. In fact, the miniGs heterotrimer engages strong and specific interaction with IBS residues, locking A2A in its *active* state, as shown by the RMSD comparison (Supplementary Fig. S2) between the two *coupled* systems (*FANG* and *FApoG*) with the corresponding *uncoupled* ones (*FAN* and *FApo*).

Interestingly, allosteric communications between the OBS and the IBS have been found looking at the motion of the intracellular receptor region in the *holo Gs-uncoupled* systems (FAN, INeca and INzma). In fact, in such cases the RMSD of the IBS is lower, in terms of both values and fluctuations, compared to the two *apo Gs-uncoupled* trajectories (*FApo* and *INapo*). This finding suggests that the A2A's intracellular portion can be stabilised by the binding of a specific

ligand to OBS, in addition to the stability given by the binding of transducers at IBS. In this perspective, we investigated the presence of correlated A2A inter-helical motions in the different simulated systems by computing a Pearson Coefficient (PC) matrix (Supplementary Fig. S3). Interestingly, this analysis confirmed that the overall receptor dynamics is strongly reduced when either the orthosteric ligand or G protein - or both - are bound to the GPCR. Indeed, looking at the PC maps (Fig. S3) few spots at positive (blue spots, PC > 0.5) or negative (red spots, PC > 0.5) correlation values are found in all the *holo/coupled* systems, whereas significant inter-helical communication areas were observed in the *apo-uncoupled* systems *INapo* and *FApo*. Particularly, a tight coupling between the motions of TM6 and either TM3-TM4 or TM1-TM2 is observed in *FApo* (Supplementary Fig. S3), in agreement with the RMSD values computed of the receptor's TMs and the connector region that highlight the largest conformational changes for the *FApo* receptor state among all the simulated systems (Supplementary Fig. S4 and S5, respectively).

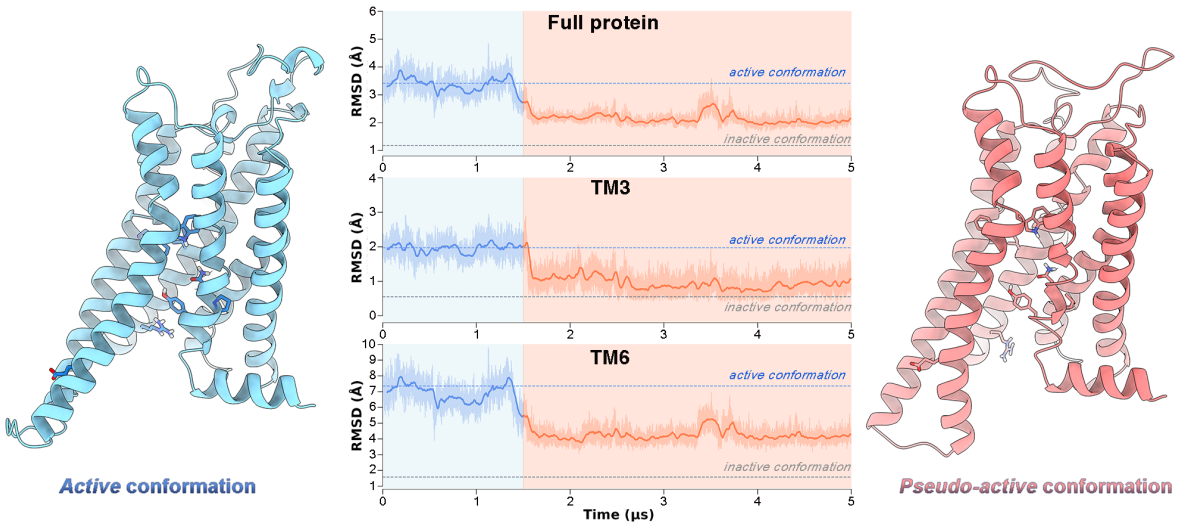

Figure 2. *Active* to *pseudo-active* transition observed on the Active Apo (*FApo*) A2AR system. The RMSD plots computed with respect to the inactive A2A conformation for the entire protein and for the TM3 and TM6 helices (Cα atoms) are shown in the centre. On the sides, the tridimensional structures of the starting full active conformation (light blue cartoon) and of the newly identified *pseudo-active* state (coral cartoon).

Indeed, within ~1.6 µs the *apo G protein uncoupled* A2A undergoes a major conformational rearrangement of TM3 and TM6, moving from its starting active state towards the inactive one (Fig. 2). Such large-scale motion is characterised by two main events. In the first one, the two helices move in opposite directions along the axis perpendicular to the membrane plane (z), with TM3 shifting downward (intracellularly) and TM6 upward (extracellularly) of ~3 Å. In the second one, the intracellular segment of TM6 approaches the centre of the TM bundle, assuming a state-specific tilted conformation (Fig. 2). This represents the final state of the receptor that is stable for the rest of the simulation time, longer than 3.4 µs Supplementary Fig. S6). The newly identified A2A state, hereafter referred to as *pseudo-active state* (pAS), has never been characterised before and its remarkable structural and energetic stability prompted us to deeply analyse this receptor conformation in the following section.

Structure of A2A pAS

The tridimensional structure of the newly identified A2A pAS is rather different from both the *inactive* (ZMA-bound, PDB code: 4UM9) and *active* (NECA and G protein-bound, PDB code: 5G53) states, with RMSD values computed for the backbone C-α atoms of 2.52 Å *vs.* 3.28 Å, respectively. A closer inspection of the structure reveals the key residues that stabilise this receptor conformation as transition intermediate between the active and inactive form. Such residues were identified by analysing the *FApo* A2A conformations collected during the MD simulation through a Protein Structure Network (PSN) model that is able to assess time-related residue-residue interactions (see Supplementary discussion and Supplementary Fig. S4 for details). Special attention was dedicated to the analysis of residues known as "activation microswitches" in Class A GPCRs[36,58–61]. For the sake of clarity, the following discussion is organised treating separately the three main structural components of GPCRs: the OBS, the connector and the IBS regions.

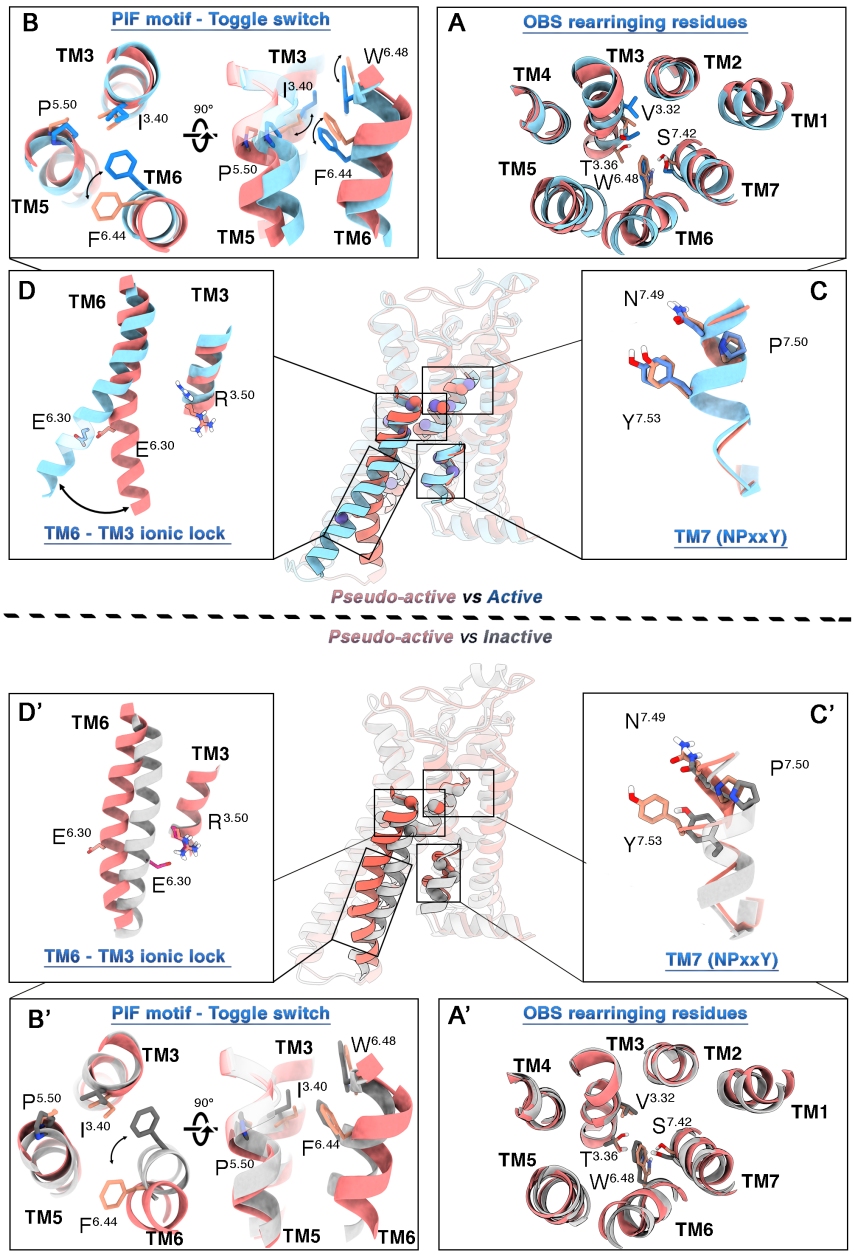

Figure 3. A virtual microscope on the structure of the intermediate state (color: coral) discovered along the *FApo* MD simulation. Comparisons with the full active A2A conformation (PDB code: 5G53, color: light blue) and with

the antagonist-induced inactive conformation (PDB code: 3PWH, color: silver) are showed in the upper part and in the bottom part, respectively. The most known (de)activation microswitches in Class A GPCRs are highlighted as sticks in the insets.

Orthosteric Binding Site (OBS). In this region, pAS is more similar to the inactive conformation than the active one. Proof of that is the lower RMSD values computed for the OBS residues in pAS with respect to those of the inactive and the active state, 0.9 and 1.25 Å, respectively. This evidence is further confirmed by analysing the conformations of the OBS residues known to be involved in receptor activation such as V84$^{3.32}$, T88$^{3.36}$, S277$^{7.42}$ and W246$^{6.48}$.[68,69,71–73] In fact, such amino acids occupy a very similar position to that observed in the inactive receptor (Fig. 3A'), while major differences occur with respect to the active conformation (Fig. 3A). In more detail, the sidechains of T88$^{3.36}$ and S277$^{7.42}$ in pAS are oriented outwards the binding site if compared to their position in the experimental active A2AR structures (Fig. 3A). In fact, in the latter structures these two residues engage polar interactions with the agonists' ribose ring, which are instead missing when the receptor is either in its apo form or bound to antagonists/inverse agonists.[68,69,72–74]Also the rotameric state of V84$^{3.32}$ and W246$^{6.48}$ ("toggle switch") is more similar to the inactive conformation than the active one in which the agonist's ribose ring shifts V84$^{3.32}$ and W246$^{6.48}$ towards an outward and downward conformation, respectively (Fig. 3A-B).

Connector Region. At variance with the OBS, the conformation assumed by the pAS connector region is state specific, dissimilar from both the active and the inactive states - RMSD values of 2.3Å and 2.4 Å, respectively - and is characterized by a distinctive orientation of the PIF motif. Comparing pAS to the active A2A, TM6 shows an upward movement along the z axis and a counterclockwise rotation, which orients the F242$^{6.44}$ sidechain outwards with respect to the active and inactive structures (Fig. 3B-B'). On the other hand, TM3 is shifted downwards, with I92$^{3.40}$ assuming its inactive state position (Fig. 3B'). This is an unprecedent finding in the context of the A2A (de)activation mechanism. In fact, in all the structural studies reported so far, TM6 was found to move inward and rotate clockwise when passing from the active to the inactive A2AR. [60,68,69,72–74] Instead in pAS, TM6 moves in the opposite direction and is rotated counterclockwise to facilitate the vertical motion of TM3 and the onset of the deactivation process.

Intracellular Binding Site (IBS). The intracellular portion of pAS is characterised by a bending of TM6. Specifically, the cytoplasmic end of TM6 is bent towards the centre of the TM bundle (Fig. 2,3C'), reducing the volume of the IBS to values comparable to that of the inactive A2A X-ray structure (Supplementary Fig. S7). However, two major differences arise by comparing the pAS and the inactive-state IBSs. First, the middle-lower portion of TM6 (residues 229-237) is slightly shifted outwards (Fig. 3C'). This might be due to the steric hindrance of the NPxxY motif at TM7 in the pAS. In fact, such motif assumes a position very similar to that of the *active* A2A (Fig. 3D), directly interacting with TM5 through the known water-bridged H-bond between Y288$^{7.53}$ and Y197$^{5.58}$.[61] The second relevant feature is that TM6 is rotated about 40°-50° counterclockwise with respect to the inactive state (Fig. 3D'). This conformation is stabilised by a salt-bridge interaction between R205$^{5.66}$ of TM5 and E228$^{6.30}$ of TM6. Noteworthily, the same interaction can be found in the active state structures of Rhodopsin and A3A adenosine receptors (Fig. 4A).[42,75] Our simulations results show that such ionic interaction is very stable in all the A2A structures with TM6 in an active-like rotameric state (frequency of occurrence > 95%, Fig. 4B), whereas it is lost in all the A2AR inactive conformations (Fig. 4B). In the latter, E228$^{6.30}$ is oriented toward the inner part of the IBS and interacts with R102$^{3.50}$ of the DRY motif, forming the "inactivating ionic lock" (IIL). Interestingly, R205$^{5.66}$ and E228$^{6.30}$ are highly conserved among the Class A GPCRs (37% and 35%, respectively, Fig. 4C), prompting us to propose the E228$^{6.30}$-R205$^{5.66}$ salt-bridge as the "activating ionic lock" (AIL), *alter ego* of the IIL, whose loss facilitates the clockwise rotation of TM6 and in turn the deactivation process.

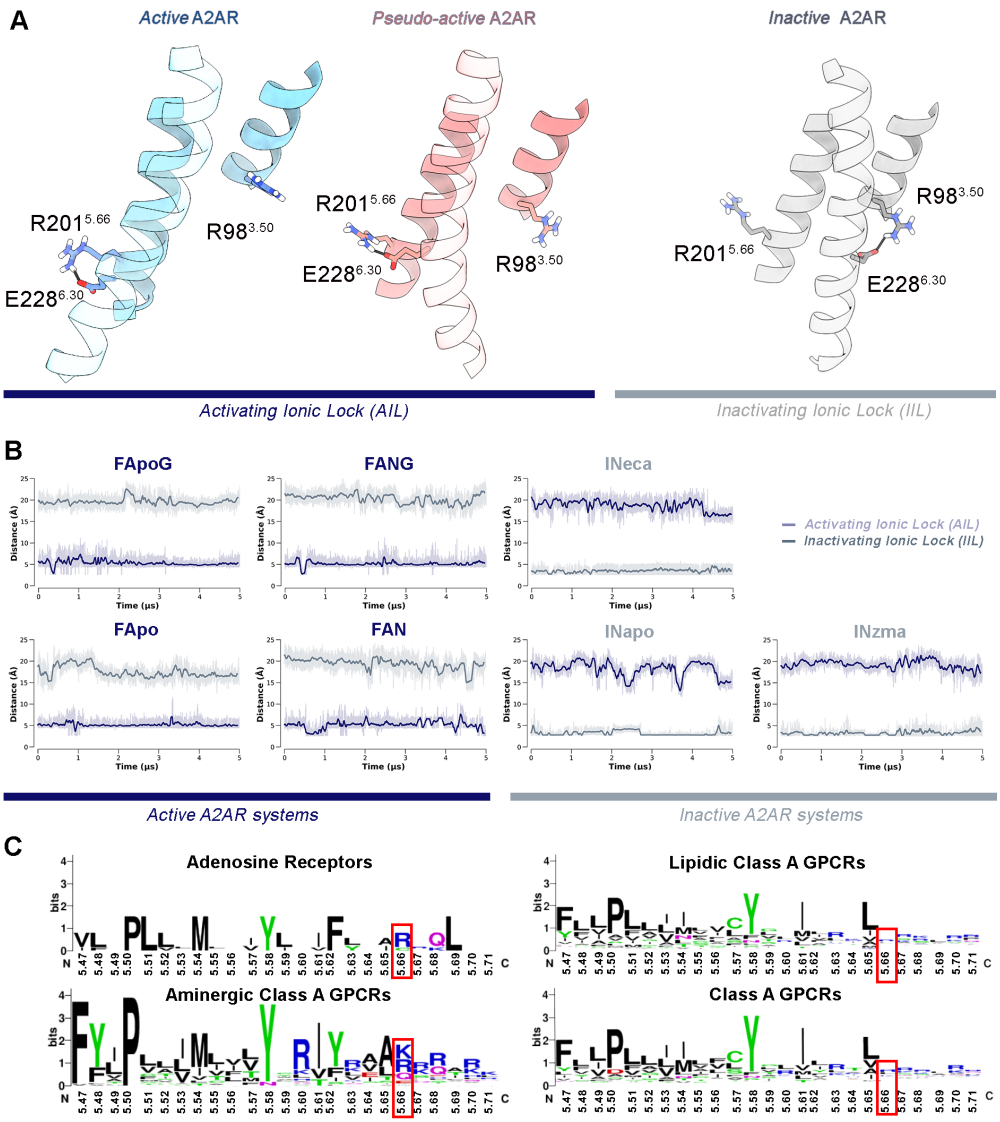

Figure 4. A) 3D representation of the activating ionic lock (AIL) and inactivating ionic lock (IIL) in the A2A's active, pseudo-active and inactive states. The helices TM3, TM4 and TM6 are depicted as cartoon while residues E288$^{6.30}$, R201$^{5.66}$ and R98$^{3.50}$ are highlighted as sticks. B) Plots of the AIL and IIL distances (E288$^{6.30}$ (cγ) –R201$^{5.66}$ (cζ) and E288$^{6.30}$ (cγ) – R98$^{6.30}$ (cζ), respectively) along the seven MD systems. C) LOGOs analysis of residues 181$^{5.47}$-206$^{5.71}$ of TM5. The conservation percentages for basic aminoacids at position 5.66 in the four investigated subsets (Adenosine, Aminergic, Lipidic and entire Class A) of Class A GPCRs are respectively: 75%, 68%, 38% and 37%.

Our findings prompted us to further investigate the role of the new pAS along the A2A transition from the active to the inactive state by analysing the MD simulations of the *apo GP-uncoupled* A2A. Our results show that pAS can be reached from the active state (*FApo* system), but not from the inactive one (*INapo* system), which is instead stable throughout the simulation (Supplementary Fig. S4). Furthermore, pAS is a very stable, long-lasting sate with a residence time longer than 3 µs (Supplementary Fig. S6). This finding indicates that pAS is a metastable, intermediate state between the active and inactive state, which are separated by a relatively large energy barrier that cannot be crossed within microsecond (simulation) timescale. Our results further show that in absence of the orthosteric ligand and G protein, the receptor tends to the inactive state, in agreement with NMR and fluorescence-based studies[11,55,76] that found the *apo* A2A in a state similar to the inverse agonist-bound conformation. In order to observe the transition between the active and inactive state, it is necessary to accelerate the sampling and overcome the timescale limitation of standard MD simulations. This is possible by employing enhanced sampling calculations based on Well-Tempered

Metadynamics (WT-MetaD)[77,78] combined with Path Collective Variables (PCVs) (See experimental section for details).[79] Particularly, PCV is a dimensionality reduction approach suitable to describe large-scale protein motion, taking into account multiple degrees of freedom of a system for which the terminal states are known, as in the A2A case. The process under investigation is thus accelerated by applying a bias potential along the PCV that is defined as a path composed by a sequence of intermediate conformations connecting the two terminal system's conformations (A2A active and inactive states in our case). We note that during the PCV WT-MetaD calculations the receptor can explore conformations even different from the original path, thus making the results independent from the choice of the original path. PCV-MetaD calculations have been successfully employed by us and other groups to study large scale and long timescale conformational changes in different protein systems.[80–83] In the case of A2A, the path is defined considering pAS as intermediate state between the terminal active and inactive state, and including the residues involved in the conformational transitions observed during the multi-microseconds MD calculations (see Experimental Section for details).

Activation Free Energy Landscape of A2AR

The entire (end-to-end) activation and deactivation process of A2A was investigated by means of PCV-MetaD in three different systems: i) *apo A2A; ii) NECA-bound* A2A; and iii) *ZMA-bound* A2A. In all of them, the sampling was enhanced by adding a bias potential on two PCVs, containing all the inter-residue contacts involved in the conformational receptor transitions observed in the previously discussed MD calculations (see Fig. 3 and Methods for the details). In particular, the first PCV ($_{ACT}$P) is defined as an RMSD matrix describing the geometric distance of the residues backbone atoms involved in the active-to-inactive receptor transition. The second PCV ($_{TM6}$P) is instead defined as a contact map (CMAP) between residues characterising the rotation of TM6, clockwise from active to inactive (see SI Fig X). The three free-energy calculations reached convergence at different simulation times: 2.4 μs for *apo*-A2AR, 3.5 μs for *NECA-bound*-A2AR, and 3.6 μs for *ZMA-bound*-A2AR, for a total of 9.5 μs of enhanced sampling simulations (Fig. S8-10). Considering the acceleration factor computed during the MetaD calculations (10^8-10^9), we could reasonably estimate that the A2A activation process occurs with a minute timescale. For each system, at the end of the simulation we computed the activation free-energy surface (FES) as a function of two CVs, $_{ACT}$P.s and $_{ACT}$P.z (See Methods for details). The first CV ($_{ACT}$P.s) describes the receptor exploration of the different states forming the transition path from the active to the inactive state, while the second CV ($_{ACT}$P.z) defines the distance as MSD of the sampled conformations from the reference path (Fig. 5A). As previously introduced, using PCV-MetaD the systems can explore conformations even distant from the reference path that, in such a case, would have high $_{ACT}$P.z values. Interestingly, in the three systems all the low energy minima - hence most probable receptor states - have low $_{ACT}$P.z values (< 0.5 nm). This result indicates that the reference path employed in WT-MetaD calculations well represents the low energy transition path from active to inactive A2A, leading to a reliable description of the A2A (de)activation process.

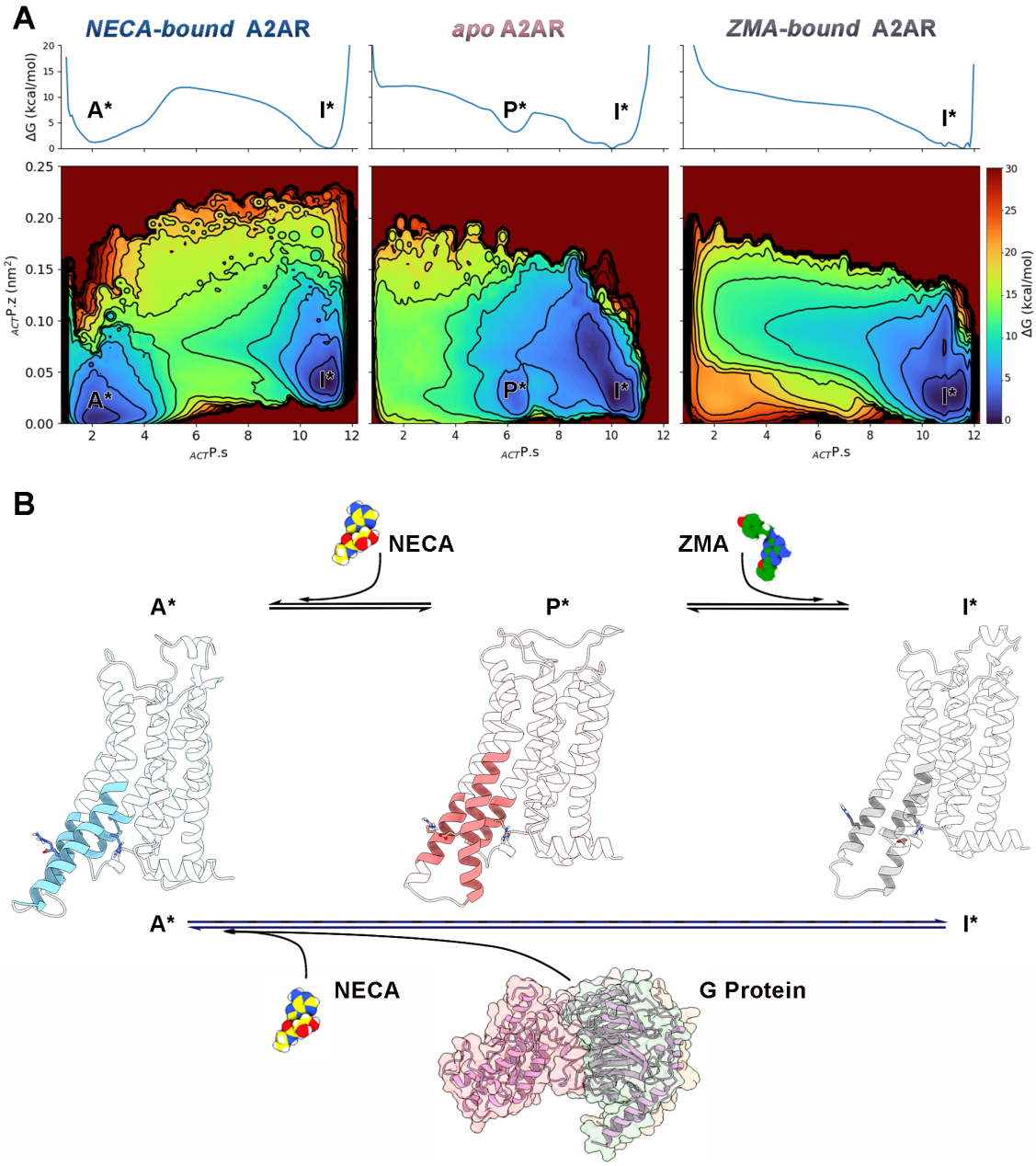

Figure 5. A) Activation Free Energy landscapes of the *NECA-bound*, *apo* and *ZMA-bound* forms of A2AR as a function of the $_{ACT}$P.s and $_{ACT}$P.z collective variables. Isosurfaces are displayed every 3 kcal/mol. B) Atomistic representation of the A2AR structures corresponding to the main free energy minima (A*,P*,I*) and equilibria interconnecting the same conformations along the activation process.

Comparing the three FESs in Fig. 5, it is possible to assess the effect of ligand binding on the low energy states assumed by the receptor during its active-to-inactive transition. In detail, the *NECA-bound* A2AR is in equilibrium between two energetically comparable states. The first, namely state A*, corresponds to the *active* crystallographic structure (RMSD = 1.4 Å), whereas the second – state I* – is very similar to the inactive receptor state (RMSD = 1.6 Å). This finding indicates that upon agonist binding i) the receptor can reach the active conformation competent for G protein binding; and ii) the inactive form remains the lowest energy receptor state in absence of G protein as detected by experimental structures. Similarly to the *NECA-bound* system, the *apo* A2A has two lowest energy conformations. While the lowest energy minimum is still represented by the A2A *inactive* conformation (state I*) (RMSD = 1.3 Å), the second energy minimum is not the active state, but state P* that corresponds to the pAs structure

previously identified by our unbiased MD calculations (RMSD < 1.2 Å). Therefore, the free-energy calculations confirm the presence of the *pseudo-active* state pAs as metastable intermediate between the active and inactive form of apo A2A. Differently, the presence of ZMA at the OBS shifts the conformational equilibrium toward the *inactive* state. In fact, the *ZMA-bound* A2A has one single low energy minimum (state I*), corresponding to the crystallographic pose of the receptor in complex with ZMA. Comparing the FESs in Fig. 5, one can see that in *ZMA-bound* A2A both the active and *pseudo-active* state are lost in favor of the inactive state. Therefore, ZMA works as inverse agonist, altering the conformational equilibrium of the apo state and locking the receptor in the inactive form. The energetic and structural stability of all the identified minima was further investigated and confirmed by over 1 μs of unbiased MD simulations performed on the corresponding states (A*, P* and I*) (Supplementary Fig. S11).

In order to characterize more deeply the mechanism of A2A activation, we computed the FES as a function of $_{ACT}$P.*s* and $_{TM6}$P.*s* (Supplementary Fig. S12). As introduced before, the $_{ACT}$P.*s* CV defines the active-to-inactive receptor transition – specifically the outward/inward motion of helices TM5-6-7 - while the second CV ($_{TM6}$P.*s*) describes the *around-the-axis* rotation of TM6 (clockwise or counter-clockwise). Looking at these FESs, the highest energy barriers are found along the $_{TM6}$P.s CV. Therefore, the TM6 rotation represents a slower degree of freedom than the TM5-6-7 outward/inward motion and can be considered the rate determining step of the (de)activation process. Three hubs of microswitch residues rule the receptor motion and are: i) the salt bridges engaged by E228$^{6.30}$ with R205$^{5.66}$ in the active form (AIL - *activating ionic lock*) and with R102$^{3.50}$ in the inactive one (IIL – *inactivating ionic lock*); ii) the Van der Waals interactions established by L235$^{6.37}$, I238$^{6.39}$, V239$^{6.40}$ with L194$^{5.55}$, L198$^{5.59}$ and F201$^{5.62}$ in the *active* and *pseudo-active* states, and with L95$^{3.43}$, I98$^{3.46}$ and I200$^{5.61}$ in the *inactive* states; and iii) the water-bridged interaction between Y197$^{5.58}$ and Y288$^{7.53}$ in both the *active* and *pseudo-active* states. The loss of the latter allows the outward motion of the NPxxY motif characterizing the receptor deactivation.

Discussion:

In this study, we have provided a thorough structural and energetics characterisation of the activation mechanism of the adenosine G protein coupled receptor A2A. Specifically, the apo, the agonist-bound and the inverse agonist-bound forms of the receptor have been investigated. Among these the A2A apo form is particularly interesting as this represents the basal functional state of the receptor for which no experimental structure has been reported so far. In this condition, the receptor can assume the inactive form, as also outlined by previous NMR and fluorescence studies[11,55,76], in equilibrium with a pseudo-active state pAS, which is here disclosed for the first time (*P*-I* equilibrium*, Figure 5B). In the pAS structure the receptor presents a mix of features – i.e., microswitch residues interactions - of the active and inactive state. The most important one is the salt bridge interaction established between E228$^{6.30}$ and R205$^{5.66}$ - largely conserved within class A GPCRs - which stabilises the TM6 active-like orientation forming what we have defined as activating ionic lock (AIL). Our finding prompted us to further investigate the potential role of the newly identified state pAS in signal transduction by performing protein-protein docking calculations with the two effector proteins Gs protein (i.e., miniGs) and β-arrestin 1. Our results revealed that the coupling of pAS with G protein is prevented by the steric hindrance of the TM6 intracellular tail (Figure SX), which significantly reduces the A2A IBS's volume (see SIFig. X). Interestingly, a high affinity is instead computed between pAS and β-arrestin 1 (Figure 6), with the obtained binding complex very similar to the Cryo-EM structure of the β1-adrenoreceptor coupled with β-arrestin 1 (Figure SY). This result indicates that pAS might selectively recruit β-arrestin 1, opening new opportunities for receptor bias signaling studies.

When A2A is bound to the agonist NECA without G protein, the receptor is found in two most probable states (*A*-I* equilibrium,* Figure 5B). The first one corresponds to the inactive structure of A2A, in agreement with the reported X-Ray and Cryo-EM ligand-bound A2A structures [72–74,84]. Specifically, although the experimental agonist-A2A (*GP-uncoupled*) complexes are usually defined as intermediate states, they all present TM6 rotated clockwise with E228$^{6.30}$ interacting with R102$^{3.50}$ (IIL - *inactivating ionic lock*), which represents an hallmark of receptor inactivation. Indeed, plotting the position of the experimental agonist-bound A2A structures[72–74,84] onto the FES of the activation mechanism, they all result very close to the inactive state I* (Figure S13). On the other hand, the second low-energy state corresponds to the receptor active form, characterised by the counterclockwise rotation of TM6 and the presence of the AIL. This receptor state rationalises the ^{19}F-NMR data of agonist-bound A2A reported by Prosser and colleagues,[55] and indicates that the agonist binding - even in absence of G protein - induces conformational changes in A2A leading to the loss of pAS in favour of the active form (*A**), which is competent for the G protein binding. Based on our results, it can be suggested that the *active-inactive (A*-I*) equilibrium* established upon agonist binding is functional for the definitive activation of the receptor - and stabilisation of the active form - occurring only after the G protein recruitment at the receptor IBS.

Finally, when the receptor is bound to ZMA, the basal *P*-I* equilibrium* is shifted towards the inactive conformation, which is the only low energy state present (Figure 5). We note that the intrinsic activity of ZMA is debated, with studies reporting this ligand as antagonist,[85–87] while more recent works attribute to ZMA an inverse agonist activity.[51,53,55] Our results indicate that ZMA works as inverse agonist, locking the receptor in the inactive form. In fact, if ZMA worked as antagonist, it should hamper the agonist binding to the OBS without altering the two-states equilibrium of the A2A apo form.

Our study provides unprecedented structural and energetics insight into A2A activation mechanism, revealing a novel receptor pseudo-active state that could be further investigated by functional biased signaling studies and targeted by drug design campaigns to develop A2A biased ligands. Our protocol has demonstrated ability in describing the full activation mechanism of GPCRs and in predicting the intrinsic activity of ligands based on their effect on the receptor conformational dynamics, thus representing a precious tool for GPCRs investigations and drug design.

Experimental Section

Systems setup and Unbiased Molecular Dynamics

According to the best resolution criterion, the starting conformations of the active and inactive A2AR have been taken respectively from the 5G53[68] and 5IU4[88] X-ray structures, whereas the coordinates of the mini G_s heterotrimer were extracted from the cryo-EM structure 6GDG[69] (after the alignment of the GPCR section with 5G53). The *active-uncoupled* (*FAN*, *FApo*) and the *apo* (*FApo*, *FApoG* and *INapo*) systems were obtained by differently removing the engineered G protein and the co-crystalized orthosteric ligands from the original pdbs (5G53[68] and 5IU4[88]). To prepare the *INeca* system, we first aligned the agonist- and antagonist-bound A2AR, and then replaced the antagonist ZMA in the inactive receptor conformation (pdb: 5IU4[88]) with the agonist NECA. Any mutation present in the starting pdbs were converted to their wild-type form. Before MD simulations, the receptor first N-terminal (S5) and the last C-terminal (S305) residues were capped with acetyl and N-methyl groups, respectively, and missing intra-cellular loops were added and refined using Prime.[89,90] The receptor conformations were prepared using the Protein Preparation Wizard tool, implemented in the Maestro Suite 2021.[91] Correct bond orders were assigned, missing hydrogen atoms added and all the water molecules deleted from the receptor structure. Then, a prediction of the side chains ionization and tautomeric states was performed using Epik.[92,93] Finally, the receptor hydrogen-bonding network was optimized, and the position of all the hydrogens minimized. Each optimized receptor conformation was then embedded in a 105 Å x 105 Å (along x and y axes) pre-equilibrated 1-palmitoyl-2-oleoylphosphatidylcholine (POPC)—cholesterol (7:3 molar ratio) bilayer and solvated using the TIP3P water model with the aid of the membrane-builder tool of CHARMM-GUI.org (http:// www.charmm-gui.org). The ff14SB and lipid17 Amber force fields were used to parametrize the protein and the lipids, respectively.[94] As for the GPD molecule and for the two orthosteric ligands, namely NECA and ZMA, different force fields were used based on the distinct chemical nature of the three compounds. Specifically, a combination of Amber OL3[95] and gaff[96] (generalized amber force field) force fields parameters were adopted for GPD and NECA, while the gaff[96] alone was used to treat ZMA. Their atomic partial charges were instead computed using the two-stages restrained electrostatic potential (RESP)[97,98] fitting procedure implemented in Antechamber.[99] The electrostatic potentials (ESP) were first calculated through the quantomechanical package Gaussian 16.[100] Specifically, the adopted protocol included a double step geometry optimization procedure at Hartree–Fock level of theory: i) a preliminary calculation with the 3–21G basis set, followed by ii) a more accurate procedure with the 6-31G* basis set, after which the ESP potentials were computed. The topology files of the systems were obtained with the tleap program of AmbertTools20[101] and then converted into the Gromacs format by the mean of ParmEd. The GROMACS 2020.6[102] code was used to perform the simulations. A cutoff of 12 Å was used for short-range interactions. The long-range electrostatic interactions were computed through the particle mesh Ewald method[103] using a 1.0 Å grid spacing in periodic boundary conditions. The non-iterative LINCS[104] algorithm was applied to constraint bonds, which allowed using a 2 fs integration time step. To solve all the steric clashes, each system underwent 30,000 steps of steepest descent energy minimization in three phases. In the first one, the system heavy atoms were kept fixed to relax only the hydrogens and the water molecules; during the second stage also the lipidic bilayer was released; and in the third step all the atomic positions were minimized. Then, each complex was equilibrated and heated up to 300 K, alternating NPT and NVT cycles (for a total of 30 ns) with the Berendsen coupling bath and barostat,[105] while applying gradually decreasing harmonic constraints on the heavy atoms of the membrane, protein, and ligands.

For each system, production runs of 5 μs each were performed in the NPT ensemble; the pressure of 1 atm and the temperature of 300 K were kept constant with the stochastic velocity rescaling[106] and the Parrinello-Rahman[107] algorithms, respectively.

Well-Tempered Metadynamics with Path Collective Variables

Metadynamics[77] is an enhanced sampling method in which the simulation is boosted by a gaussian-shaped history-dependent bias potential (V_G), deposited on a selected number of reaction coordinates (i.e. slow degrees of freedom) of the system, usually referred to as collective variables (CVs):

$$\boldsymbol{V_G(S,t)} = \int_0^t \boldsymbol{dt'\omega} \exp - \sum_{i=1}^{d} \frac{\left(\boldsymbol{S_i(R)} - \boldsymbol{S_i(R(t'))}\right)^2}{2\boldsymbol{\sigma_i}^2} \quad (1)$$

where S_i is the value of the ith CV, σ_i is the width of the Gaussian function and ω is the rate at which the bias is deposited. Well-Tempered Metadynamics (WT-MetaD)[78] is an evolution of the method in which the bias deposition rate ω is exponentially rescaled over time depending on how much potential has already been added in the same region of the CV phase space, according to following formula:

$$W = \omega_0 \tau_G e^{-\frac{V_G(\boldsymbol{S},t)}{k_B \Delta T}} \quad (2)$$

where W is the Gaussian height, k_B is Boltzmann's constant, ω_0 is the initial energy rate, τ_G is the Gaussian deposition stride, ΔT is the fictitious temperature at which the biased CV (S) is sampled and $V_G(\boldsymbol{S}, t)$ is the bias potential accumulated in S over time t. At the end of a WT-MetaD simulation the deposited bias potential V_G asymptotically converges to the inverse value of a fraction of the free-energy $F(\boldsymbol{S})$:

$$V_G(\boldsymbol{S}, t \to \infty) = -\frac{\Delta T}{\Delta T + T} F(\boldsymbol{S}) \quad (3)$$

The fictitious temperature ΔT is the parameter that controls how quickly the Gaussian height is decreased and often is written in terms of a so-called bias factor $\gamma = (T + \Delta T)/T$.

The large-scale conformational differences between the crystal structures of the active and inactive A2AR suggest that the transition between these states is highly cooperative and involves a number of degrees of freedom. For this reason, the use of simple geometrical CVs (i.e. a distance or a torsion) might be insufficient both to reproduce the event and to calculate the associated free energy. To overcome this limitation, we employed the path collective variables (PCVs) approach[79], which has been successfully applied in a number of conformational transition studies.[80–83] In this dimensionality reduction scheme, two functions are used to characterize the position of a point in a configurational space **R** relative to a preassigned path $\boldsymbol{l}$ in terms of progress along the path $s(\mathbf{R})$ and distance from it $z(\mathbf{R})$:

$$s(\mathbf{R}) = \frac{1}{N-1} \frac{\sum_{i=1}^{N} (i-1)\, exp(-\lambda \|X(\mathbf{R}) - X(\boldsymbol{l})\|^2)}{\sum_{i=1}^{N} exp(-\lambda \|X(\mathbf{R}) - X(\boldsymbol{l})\|^2)} \quad (4)$$

$$z(\mathbf{R}) = -\frac{1}{\lambda} ln[\sum_{i=1}^{N} exp(-\lambda \|X(\mathbf{R}) - X(\boldsymbol{l})\|^2)] \quad (5)$$

where $X(\mathbf{R})$ is a reduced representation of **R**, $X(\boldsymbol{l})$ is the same kind of reduced representation of the path $\boldsymbol{l}$, i is a discrete index ranging from 1 to N, with N being the number of conformations selected to build the path. ‖…‖ indicates the metric used to compute the distance between the configurations, which is generally defined in terms of contacts matrix or RMSD. In this work, a preliminary guess of the A2AR activation process was obtained through the unbiased MD system *FApo* (transition from the *active* to the *pseudo-active* state) and targeted-MD (transition from the *pseudo-active* state to the *inactive* state). The latter was performed applying a constant force (harmonic constant k =

20.000 kJ/mol) on a collective variable represented by the RMSD of the protein Cα atoms computed with respective to the experimental inactive conformation of A2AR. The overall trajectory was then used to extract the frames needed for the preassigned paths of two sets of PCVs: P_{ACT} and P_{TM6}.

***P_{ACT}* Collective Variable:** In S_{ACT}, $X(\mathbf{R})$ is defined as a set of Cartesian coordinates belonging to a subset of atoms. The distance ‖…‖ of each generic configuration $X(\mathbf{R})$ from the path was computed as the root mean square displacement (RMSD) of the subset after optimal receptors alignment by using Kearsley's algorithm[108]. Notably, the choice of the atoms to be included in the path is far from trivial, in fact, a wrong choice can turn into a loss of performance and additional noise that may affect the calculations. Here, we used the Cα and Cβ of the most important receptor microswitches (PIF, toggle, NPxxY, AIL, IIL) as well as the Cζ and Cγ of key residues detected in our unbiased MD (Table S1). The final path consists of 12 frames: 10 frames directly extracted from the preliminary deactivation trajectory (obtained as described above), and two terminal extra-(non-real)-frames. We verified that the obtained set of configurations was equally spaced in the adopted mean square displacement metrics, and the value of λ was chosen so as to be comparable to the inverse of the RMSD between successive frames. The average distance between adjacent frames was 0.74 Å, thus requiring to set λ = 1.22 $Å^{-2}$ in eqs 2 and 3.

***P_{TM6}* Collective Variable:** Here, the reduced representation $X(\mathbf{R})$ is defined as the CMAP matrix $C(\mathbf{R})$, and the distance ‖…‖ computed as:

$$\|X(\mathbf{R}) - X(l)\| = \sum_{j>1}\left[C(\mathbf{R})_{i,j} - C(\boldsymbol{l})_{i,j}\right]^2 \tag{6}$$

where $C(\mathbf{R})_{i,j}$ and $C(\boldsymbol{l})_{i,j}$ are the elements of the CMAP matrix. A contact between atom *i* and *j* is defined as

$$\mathrm{C}(\mathbf{R})_{i,j} = \frac{1-\left(\frac{r_{ij}}{r_0}\right)^n}{1-\left(\frac{r_{ij}}{r_0}\right)^m} \tag{7}$$

where $r_{i,j}$ is the distance between the two atoms and r_0 is the typical distance at which the contact is formed (SI Text). The list of the contacts included (Table S2) in the CV was chosen to specifically accelerate the around-the-axis rotation of TM6 occurring upon receptor (de)activation. The final path consists of 9 frames: 7 frames directly extracted from the preliminary deactivation trajectory, and two terminal extra-(non-real)-frames. The average distance between adjacent frames was 0.63, thus requiring to set λ = 3.64 according to the same criterion used for S_{ACT}.

The PLUMED 2.7.1[109,110] library patched with the Gromacs 2020.6[102] MD engine was used to perform WT-MetaD simulations on the uncoupled A2AR in its *apo*, *NECA-bound* and *ZMA-bound* forms. Two-dimensional gaussians were added on the $s(\mathbf{R})$ components of P_{ACT} *and* P_{TM6} every 2 ps. An initial gaussian height of 4 kJ/mol was gradually decreased based on a bias factor γ = 15. The gaussian widths were respectively set to 0.1 and 0.03 for the $P.s_{ACT}$ and for $P.s_{TM6}$ dimensions according to the CVs' fluctuations observed in the standard MD regime. To limit the exploration of unphysical states during the simulations harmonic restraints were placed on the helicity of TM6, based on the ALPHARMSD variable defined in PLUMED. The bias reweighting procedures used along this work were performed according to the algorithm developed by Bonomi et al.[111]

References

(1) Rosenbaum, D. M.; Rasmussen, S. G. F.; Kobilka, B. K. The Structure and Function of G-Protein-Coupled Receptors. *Nature* **2009**, *459*, 356–363.

(2) Yang, D.; Zhou, Q.; Labroska, V.; Qin, S.; Darbalaei, S.; Wu, Y.; Yuliantie, E.; Xie, L.; Tao, H.; Cheng, J.; Liu, Q.; Zhao, S.; Shui, W.; Jiang, Y.; Wang, M. W. G Protein-Coupled Receptors: Structure- and Function-Based Drug Discovery. *Signal Transduct. Target. Ther.* **2021**, *6*.

(3) Hilger, D.; Masureel, M.; Kobilka, B. K. Structure and Dynamics of GPCR Signaling Complexes. *Nat. Struct. Mol. Biol.* **2018**, *25*, 4–12.

(4) Weis, W. I.; Kobilka, B. K. The Molecular Basis of G Protein-Coupled Receptor Activation. *Annu. Rev. Biochem.* **2018**, *87*, 897–919.

(5) Hauser, A. S.; Kooistra, A. J.; Munk, C.; Heydenreich, F. M.; Veprintsev, D. B.; Bouvier, M.; Babu, M. M.; Gloriam, D. E. GPCR Activation Mechanisms across Classes and Macro/Microscales. *Nat. Struct. Mol. Biol.* **2021**, *28*, 879–888.

(6) Venkatakrishnan, A. J.; Deupi, X.; Lebon, G.; Tate, C. G.; Schertler, G. F.; Madan Babu, M. Molecular Signatures of G-Protein-Coupled Receptors. *Nature* **2013**, *494*, 185–194.

(7) Manglik, A.; Kruse, A. C. Structural Basis for G Protein-Coupled Receptor Activation. *Biochemistry* **2017**, *56*, 5628–5634.

(8) Rasmussen, S. G. F.; Choi, H. J.; Fung, J. J.; Pardon, E.; Casarosa, P.; Chae, P. S.; Devree, B. T.; Rosenbaum, D. M.; Thian, F. S.; Kobilka, T. S.; Schnapp, A.; Konetzki, I.; Sunahara, R. K.; Gellman, S. H.; Pautsch, A.; Steyaert, J.; Weis, W. I.; Kobilka, B. K. Structure of a Nanobody-Stabilized Active State of the B2 Adrenoceptor. *Nature* **2011**, *469*, 175–181.

(9) Rosenbaum, D. M.; Zhang, C.; Lyons, J. A.; Holl, R.; Aragao, D.; Arlow, D. H.; Rasmussen, S. G. F.; Choi, H. J.; Devree, B. T.; Sunahara, R. K.; Chae, P. S.; Gellman, S. H.; Dror, R. O.; Shaw, D. E.; Weis, W. I.; Caffrey, M.; Gmeiner, P.; Kobilka, B. K. Structure and Function of an Irreversible Agonist-B2 Adrenoceptor Complex. *Nature* **2011**, *469*, 236–242.

(10) Smith, J. S.; Lefkowitz, R. J.; Rajagopal, S. Biased Signalling: From Simple Switches to Allosteric Microprocessors. *Nat. Rev. Drug Discov.* **2018**, *17*, 243–260.

(11) Prosser, R. S.; Ye, L.; Pandey, A.; Orazietti, A. Activation Processes in Ligand-Activated G Protein-Coupled Receptors: A Case Study of the Adenosine A2A Receptor. *BioEssays* **2017**, *39*, 1–10.

(12) Warne, T.; Edwards, P. C.; Dorfe, A. S.; Leslie, A. G. W.; Tate, C. G. Molecular Basis for High-Affinity Agonist Binding in GPCRs. *Science (80-.).* **2019**, *778*, 775–778.

(13) Neves, S. R.; Ram, P. T.; Iyengar, R. G Protein Pathways. *Science (80-.).* **2002**, *296*, 1636–1639.

(14) Oldham, W. M.; Hamm, H. E. Heterotrimeric G Protein Activation by G-Protein-Coupled Receptors. *Nat. Rev. Mol. Cell Biol.* **2008**, *9*, 60–71.

(15) Hurowitz, E. H.; Melnyk, J. M.; Chen, Y. J.; Kouros-Mehr, H.; Simon, M. I.; Shizuya, H. Genomic Characterization of the Human Heterotrimeric G Protein α, β, and γ Subunit Genes. *DNA Res.* **2000**, *7*, 111–120.

(16) Krasel, C.; Lohse, M. J. G Protein Coupled Receptor Kinases. *xPharm Compr. Pharmacol. Ref.* **2007**, 1–19.

(17) McGarrigle, D.; Huang, X. Y. GPCRs Signaling Directly through Src-Family Kinases. *Sci. STKE* **2007**, *2007*, 1–4.

(18) Smith, J. S.; Rajagopal, S. The β-Arrestins: Multifunctional Regulators of G Protein-Coupled Receptors. *J.*

Biol. Chem. **2016**, *291*, 8969–8977.

(19) Shiraishi, Y.; Kofuku, Y.; Ueda, T.; Pandey, S.; Dwivedi-Agnihotri, H.; Shukla, A. K.; Shimada, I. Biphasic Activation of β-Arrestin 1 upon Interaction with a GPCR Revealed by Methyl-TROSY NMR. *Nat. Commun.* **2021**, *12*, 1–7.

(20) Slosky, L. M.; Caron, M. G.; Barak, L. S. Biased Allosteric Modulators: New Frontiers in GPCR Drug Discovery. *Trends Pharmacol. Sci.* **2021**, *42*, 283–299.

(21) Franco, R.; Rivas-Santisteban, R.; Reyes-Resina, I.; Navarro, G. The Old and New Visions of Biased Agonism Through the Prism of Adenosine Receptor Signaling and Receptor/Receptor and Receptor/Protein Interactions. *Front. Pharmacol.* **2021**, *11*, 1–6.

(22) Wootten, D.; Christopoulos, A.; Marti-Solano, M.; Babu, M. M.; Sexton, P. M. Mechanisms of Signalling and Biased Agonism in G Protein-Coupled Receptors. *Nat. Rev. Mol. Cell Biol.* **2018**, *19*, 638–653.

(23) Hauser, A. S.; Attwood, M. M.; Rask-Andersen, M.; Schiöth, H. B.; Gloriam, D. E. Trends in GPCR Drug Discovery: New Agents, Targets and Indications. *Nat. Rev. Drug Discov.* **2017**, *16*, 829–842.

(24) Cooray, S. N.; Gobbetti, T.; Montero-Melendez, T.; McArthur, S.; Thompson, D.; Clark, A. J. L.; Flower, R. J.; Perretti, M. Ligand-Specific Conformational Change of the G-Protein-Coupled Receptor ALX/FPR2 Determines Proresolving Functional Responses. *Proc. Natl. Acad. Sci. U. S. A.* **2013**, *110*, 18232–18237.

(25) Wingler, L. M.; Skiba, M. A.; McMahon, C.; Staus, D. P.; Kleinhenz, A. L. W.; Suomivuori, C. M.; Latorraca, N. R.; Dror, R. O.; Lefkowitz, R. J.; Kruse, A. C. Angiotensin and Biased Analogs Induce Structurally Distinct Active Conformations within a GPCR. *Science (80-.).* **2020**, *367*, 888–892.

(26) Slosky, L. M.; Bai, Y.; Toth, K.; Ray, C.; Rochelle, L. K.; Badea, A.; Chandrasekhar, R.; Pogorelov, V. M.; Abraham, D. M.; Atluri, N.; Peddibhotla, S.; Hedrick, M. P.; Hershberger, P.; Maloney, P.; Yuan, H.; Li, Z.; Wetsel, W. C.; Pinkerton, A. B.; Barak, L. S.; Caron, M. G. β-Arrestin-Biased Allosteric Modulator of NTSR1 Selectively Attenuates Addictive Behaviors. *Cell* **2020**, *181*, 1364-1379.e14.

(27) Gurevich, V. V.; Gurevich, E. V. Biased GPCR Signaling: Possible Mechanisms and Inherent Limitations. *Pharmacol. Ther.* **2020**, *211*, 107540.

(28) Wisler, J. W.; Rockman, H. A.; Lefkowitz, R. J. Biased G Protein-Coupled Receptor Signaling: Changing the Paradigm of Drug Discovery. *Circulation* **2018**, *137*, 2315–2317.

(29) Poulie, C. B. M.; Pottie, E.; Simon, I. A.; Harpsøe, K.; D'Andrea, L.; Komarov, I. V.; Gloriam, D. E.; Jensen, A. A.; Stove, C. P.; Kristensen, J. L. Discovery of β-Arrestin-Biased 25CN-NBOH-Derived 5-HT2AReceptor Agonists. *J. Med. Chem.* **2022**, *65*, 12031–12043.

(30) Wall, M. J.; Hill, E.; Huckstepp, R.; Barkan, K.; Deganutti, G.; Leuenberger, M.; Preti, B.; Winfield, I.; Carvalho, S.; Suchankova, A.; Wei, H.; Safitri, D.; Huang, X.; Imlach, W.; La Mache, C.; Dean, E.; Hume, C.; Hayward, S.; Oliver, J.; Zhao, F. Y.; Spanswick, D.; Reynolds, C. A.; Lochner, M.; Ladds, G.; Frenguelli, B. G. Selective Activation of Gαob by an Adenosine A1 Receptor Agonist Elicits Analgesia without Cardiorespiratory Depression. *Nat. Commun.* **2022**, *13*.

(31) Faouzi, A.; Wang, H.; Zaidi, S. A.; DiBerto, J. F.; Che, T.; Qu, Q.; Robertson, M. J.; Madasu, M. K.; El Daibani, A.; Varga, B. R.; Zhang, T.; Ruiz, C.; Liu, S.; Xu, J.; Appourchaux, K.; Slocum, S. T.; Eans, S. O.; Cameron, M. D.; Al-Hasani, R.; Pan, Y. X.; Roth, B. L.; McLaughlin, J. P.; Skiniotis, G.; Katritch, V.; Kobilka, B. K.; Majumdar, S. Structure-Based Design of Bitopic Ligands for the μ-Opioid Receptor. *Nature* **2023**, *613*, 767–774.

(32) Hurtley, S. M. Continuing the Resolution Revolution. *Science (80-.).* **2018**, *360*, 282.

(33) Lu, S.; He, X.; Yang, Z.; Chai, Z.; Zhou, S.; Wang, J.; Rehman, A. U.; Ni, D.; Pu, J.; Sun, J.; Zhang, J. Activation Pathway of a G Protein-Coupled Receptor Uncovers Conformational Intermediates as Targets for Allosteric Drug Design. *Nat. Commun.* **2021**, *12*, 1–15.

(34) Suomivuori, C. M.; Latorraca, N. R.; Wingler, L. M.; Eismann, S.; King, M. C.; Kleinhenz, A. L. W.; Skiba, M. A.; Staus, D. P.; Kruse, A. C.; Lefkowitz, R. J.; Dror, R. O. Molecular Mechanism of Biased Signaling in a Prototypical G Protein-Coupled Receptor. *Science (80-.).* **2020**, *367*, 881–887.

(35) Dror, R. O.; Arlow, D. H.; Maragakis, P.; Mildorf, T. J.; Pan, A. C.; Xu, H.; Borhani, D. W.; Shaw, D. E. Activation Mechanism of the β 2-Adrenergic Receptor. *Proc. Natl. Acad. Sci. U. S. A.* **2011**, *108*, 18684–18689.

(36) Latorraca, N. R.; Venkatakrishnan, A. J.; Dror, R. O. GPCR Dynamics: Structures in Motion. *Chem. Rev.* **2017**, *117*, 139–155.

(37) Hollingsworth, S. A.; Dror, R. O. Molecular Dynamics Simulation for All. *Neuron* **2018**, *99*, 1129–1143.

(38) Burg, J. S.; Ingram, J. R.; Venkatakrishnan, A. J.; Jude, K. M.; Dukkipati, A.; Feinberg, E. N.; Angelini, A.; Waghray, D.; Dror, R. O.; Ploegh, H. L.; Garcia, K. C. Structural Basis for Chemokine Recognition and Activation of a Viral G Protein-Coupled Receptor. *Science (80-.).* **2015**.

(39) Pan, A. C.; Borhani, D. W.; Dror, R. O.; Shaw, D. E. Molecular Determinants of Drug-Receptor Binding Kinetics. *Drug Discov. Today* **2013**, *18*, 667–673.

(40) Provasi, D.; Bortolato, A.; Filizola, M. Exploring Molecular Mechanisms of Ligand Recognition by Opioid Receptors with Metadynamics. *Biochemistry* **2009**, *48*, 10020–10029.

(41) Provasi, D.; Artacho, M. C.; Negri, A.; Mobarec, J. C.; Filizola, M. Ligand-Induced Modulation of the Free-Energy Landscape of G Protein-Coupled Receptors Explored by Adaptive Biasing Techniques. *PLoS Comput. Biol.* **2011**, *7*.

(42) Provasi, D.; Filizola, M. Putative Active States of a Prototypic G-Protein-Coupled Receptor from Biased Molecular Dynamics. *Biophys. J.* **2010**, *98*, 2347–2355.

(43) Fanelli, F.; Felline, A.; Raimondi, F.; Seeber, M. Structure Network Analysis to Gain Insights into GPCR Function. *Biochem. Soc. Trans.* **2016**, *44*, 613–618.

(44) Kohlhoff, K. J.; Shukla, D.; Lawrenz, M.; Bowman, G. R.; Konerding, D. E.; Belov, D.; Altman, R. B.; Pande, V. S. Cloud-Based Simulations on Google Exacycle Reveal Ligand Modulation of GPCR Activation Pathways. *Nat. Chem.* **2014**, *6*, 15–21.

(45) Sun, X.; Singh, S.; Blumer, K. J.; Bowman, G. R. Simulation of Spontaneous G Protein Activation Reveals a New Intermediate Driving GDP Unbinding. *Elife* **2018**, *7*, 1–24.

(46) Li, J.; Jonsson, A. L.; Beuming, T.; Shelley, J. C.; Voth, G. A. Ligand-Dependent Activation and Deactivation of the Human Adenosine A 2A Receptor. *J. Am. Chem. Soc.* **2013**, *135*, 8749–8759.

(47) Mafia, A.; Kima, S.-K.; William A. Goddard III. The Mechanism for Ligand Activation of the GPCR-Protein Complex. *Proc. Natl. Acad. Sci.* **2022**, *119*, 18.

(48) Wang, J.; Bhattarai, A.; Do, H. N.; Akhter, S.; Miao, Y. Molecular Simulations and Drug Discovery of Adenosine Receptors. *Molecules* **2022**, *27*, 2054.

(49) Saleh, N.; Saladino, G.; Gervasio, F. L.; Clark, T. Investigating Allosteric Effects on the Functional Dynamics of B2-Adrenergic Ternary Complexes with Enhanced-Sampling Simulations. *Chem. Sci.* **2017**, *8*, 4019–4026.

(50) Mafi, A.; Kim, S. K.; Goddard, W. A. The Dynamics of Agonist-B2-Adrenergic Receptor Activation

Induced by Binding of GDP-Bound Gs Protein. *Nat. Chem.* **2023**.

(51) Ye, L.; Van Eps, N.; Zimmer, M.; Ernst, O. P.; Scott Prosser, R. Activation of the A 2A Adenosine G-Protein-Coupled Receptor by Conformational Selection. *Nature* **2016**, *533*, 265–268.

(52) Ye, L.; Neale, C.; Sljoka, A.; Lyda, B.; Pichugin, D.; Tsuchimura, N.; Larda, S. T.; Pomès, R.; García, A. E.; Ernst, O. P.; Sunahara, R. K.; Prosser, R. S. Mechanistic Insights into Allosteric Regulation of the A2A Adenosine G Protein-Coupled Receptor by Physiological Cations. *Nat. Commun.* **2018**, *9*.

(53) Huang, S. K.; Almurad, O.; Pejana, R. J.; Morrison, Z. A.; Pandey, A.; Picard, L. P.; Nitz, M.; Sljoka, A.; Prosser, R. S. Allosteric Modulation of the Adenosine A2A Receptor by Cholesterol. *Elife* **2022**, *11*, 1–24.

(54) Fernandes, D. D.; Neale, C.; Gomes, G. N. W.; Li, Y.; Malik, A.; Pandey, A.; Orazietti, A. P.; Wang, X.; Ye, L.; Scott Prosser, R.; Gradinaru, C. C. Ligand Modulation of the Conformational Dynamics of the A2A Adenosine Receptor Revealed by Single-Molecule Fluorescence. *Sci. Rep.* **2021**, *11*, 1–16.

(55) Huang, S. K.; Pandey, A.; Tran, D. P.; Villanueva, N. L.; Kitao, A.; Sunahara, R. K.; Sljoka, A.; Prosser, R. S. Delineating the Conformational Landscape of the Adenosine A2A Receptor during G Protein Coupling. *Cell* **2021**, *184*, 1884-1894.e14.

(56) Ferré, G.; Anazia, K.; Silva, L. O.; Thakur, N.; Ray, A. P.; Eddy, M. T. Global Insights into the Fine Tuning of Human A2AAR Conformational Dynamics in a Ternary Complex with an Engineered G Protein Viewed by NMR. *Cell Rep.* **2022**, *41*.

(57) Ballesteros, J. A.; Weinstein, H. Integrated Methods for the Construction of Three-Dimensional Models and Computational Probing of Structure-Function Relations in G Protein-Coupled Receptors. *Methods Neurosci.* **1995**, *25*, 366–348.

(58) Schneider, E. H.; Schnell, D.; Strasser, A.; Dove, S.; Seifert, R. Impact of the DRY Motif and the Missing "Ionic Lock" on Constitutive Activity and G-Protein Coupling of the Human Histamine H 4 Receptor. *J. Pharmacol. Exp. Ther.* **2010**, *333*, 382–392.

(59) Vogel, R.; Mahalingam, M.; Lüdeke, S.; Huber, T.; Siebert, F.; Sakmar, T. P. Functional Role of the "Ionic Lock"-An Interhelical Hydrogen-Bond Network in Family A Heptahelical Receptors. *J. Mol. Biol.* **2008**, *380*, 648–655.

(60) Doré, A. S.; Robertson, N.; Errey, J. C.; Ng, I.; Hollenstein, K.; Tehan, B.; Hurrell, E.; Bennett, K.; Congreve, M.; Magnani, F.; Tate, C. G.; Weir, M.; Marshall, F. H. Structure of the Adenosine A2A Receptor in Complex with ZM241385 and the Xanthines XAC and Caffeine. *Structure* **2011**, *19*, 1283–1293.

(61) Fleetwood, O.; Matricon, P.; Carlsson, J.; Delemotte, L. Energy Landscapes Reveal Agonist Control of G Protein-Coupled Receptor Activation via Microswitches. *Biochemistry* **2020**, *59*, 880–891.

(62) Dall'lgna, O. P.; Porciúncula, L. O.; Souza, D. O.; Cunha, R. A.; Lara, D. R. Neuroprotection by Caffeine and Adenosine A 2A Receptor Blockade of β-Amyloid Neurotoxicity. *Br. J. Pharmacol.* **2003**, *138*, 1207–1209.

(63) Effendi, W. I.; Nagano, T.; Kobayashi, K.; Nishimura, Y. Focusing on Adenosine Receptors as a Potential Targeted Therapy in Human Diseases. *Cells* **2020**, *9*, 1–36.

(64) Ruiz, M. D. L.; Lim, Y.; Zheng, J. Adenosine A2 Receptor as a Drug Discovery Target. *J. Med. Chem.* **2014**, *57*, 3623–3650.

(65) Guerrero, A. A2A Adenosine Receptor Agonists and Their Potential Therapeutic Applications. An Update. *Curr. Med. Chem.* **2018**, *25*, 3597–3612.

(66) Golembiowska, K.; Dziubina, A. Striatal Adenosine A2A Receptor Blockade Increases Extracellular

Dopamine Release Following L-DOPA Administration in Intact and Dopamine-Denervated Rats. *Neuropharmacology* **2004**, *47*, 414–426.

(67) Headrick, J. P.; Ashton, K. J.; Rose'Meyer, R. B.; Peart, J. N. Cardiovascular Adenosine Receptors: Expression, Actions and Interactions. *Pharmacol. Ther.* **2013**, *140*, 92–111.

(68) Carpenter, B.; Nehmé, R.; Warne, T.; Leslie, A. G. W.; Tate, C. G. Structure of the Adenosine A2A Receptor Bound to an Engineered G Protein. *Nature* **2016**, *536*, 104–107.

(69) García-Nafría, J.; Lee, Y.; Bai, X.; Carpenter, B.; Tate, C. G. Cryo-EM Structure of the Adenosine A2A Receptor Coupled to an Engineered Heterotrimeric G Protein. *Elife* **2018**, *7*, 1–19.

(70) Jaakola, V.-P.; Griffith, M. T.; Hanson, M. A.; Cherezov, V.; Chien, E. Y. T.; Lane, J. R.; IJzerman, A. P.; Stevens, R. C. The 2.6 Angstrom Crystal Structure of a Human A_{2A} Adenosine Receptor Bound to an Antagonist. *Science (80-.).* **2008**, *322*, 1211–1217.

(71) Lebon, G.; Warne, T.; Edwards, P. C.; Bennett, K.; Langmead, C. J.; Leslie, A. G. W.; Tate, C. G. Agonist-Bound Adenosine A2A Receptor Structures Reveal Common Features of GPCR Activation. *Nature* **2011**, *474*, 521–526.

(72) White, K. L.; Eddy, M. T.; Gao, Z. G.; Han, G. W.; Lian, T.; Deary, A.; Patel, N.; Jacobson, K. A.; Katritch, V.; Stevens, R. C. Structural Connection between Activation Microswitch and Allosteric Sodium Site in GPCR Signaling. *Structure* **2018**, *26*, 259-269.e5.

(73) Lebon, G.; Edwards, P. C.; Leslie, A. G. W.; Tate, C. G. Molecular Determinants of CGS21680 Binding to the Human Adenosine A2A Receptor. *Mol. Pharmacol.* **2015**, *87*, 907–915.

(74) Cui, M.; Zhou, Q.; Xu, Y.; Weng, Y.; Yao, D.; Zhao, S.; Song, G. Crystal Structure of a Constitutive Active Mutant of Adenosine A2A Receptor. *IUCrJ* **2022**, *9*, 333–341.

(75) Ciancetta, A.; Rubio, P.; Lieberman, D. I.; Jacobson, K. A. A3 Adenosine Receptor Activation Mechanisms: Molecular Dynamics Analysis of Inactive, Active, and Fully Active States. *J. Comput. Aided. Mol. Des.* **2019**, *33*, 983–996.

(76) Wei, S.; Thakur, N.; Ray, A. P.; Jin, B.; Obeng, S.; McCurdy, C. R.; McMahon, L. R.; Gutiérrez-de-Terán, H.; Eddy, M. T.; Lamichhane, R. Slow Conformational Dynamics of the Human A2A Adenosine Receptor Are Temporally Ordered. *Structure* **2022**, *30*, 329-337.e5.

(77) Laio, A.; Parrinello, M. Escaping Free-Energy Minima. *Proc Natl Acad Sci USA* **2002**, *99*, 12562–12566.

(78) Barducci, A.; Bussi, G.; Parrinello, M. Well-Tempered Metadynamics: A Smoothly Converging and Tunable Free-Energy Method. *Phys. Rev. Lett.* **2008**, *100*, 020603.

(79) Branduardi, D.; Gervasio, F. L.; Parrinello, M. From A to B in Free Energy Space. *J. Chem. Phys.* **2007**, *126*, 1–10.

(80) Grazioso, G.; Limongelli, V.; Branduardi, D.; Novellino, E.; De Micheli, C.; Cavalli, A.; Parrinello, M. Investigating the Mechanism of Substrate Uptake and Release in the Glutamate Transporter Homologue Glt Ph through Metadynamics Simulations. *J. Am. Chem. Soc.* **2012**, *134*, 453–463.

(81) Berteotti, A.; Cavalli, A.; Branduardi, D.; Gervasio, F. L.; Recanatini, M.; Parrinello, M. Protein Conformational Transitions: The Closure Mechanism of a Kinase Explored by Atomistic Simulations.

(82) Bonomi, M.; Branduardi, D.; Gervasio, F. L.; Parrinello, M. The Unfolded Ensemble and Folding Mechanism of the C-Terminal GB1-Hairpin.

(83) Formoso, E.; Limongelli, V.; Parrinello, M. Energetics and Structural Characterization of the Large-Scale Functional Motion of Adenylate Kinase. **2015**.

(84) Xu, F.; Wu, H.; Katritch, V.; Han, G. W.; Jacobson, K. A.; Gao, Z. G.; Cherezov, V.; Stevens, R. C. Structure of an Agonist-Bound Human A2A Adenosine Receptor. *Science (80-.).* **2011**, *332*, 322–327.

(85) Poucher, M.; Keddie, J. R.; Singh, P.; Stoggall, S. M.; Caulkett, P. W. R.; Jones, G.; Collis, G. The in Vitro Pharmacology of ZM 241385,a Potent,Non-Xanthine, A2a Selective Adenosine Receptor Antagonist. **1995**, 1096–1102.

(86) Uustare, A.; Vonk, A.; Terasmaa, A.; Fuxe, K.; Rinken, A. Kinetic and Functional Properties of [3H]ZM241385, a High Affinity Antagonist for Adenosine A2A Receptors. *Life Sci.* **2005**, *76*, 1513–1526.

(87) Pugliese, A. M.; Traini, C.; Cipriani, S.; Gianfriddo, M.; Mello, T.; Giovannini, M. G.; Galli, A.; Pedata, F. The Adenosine A 2A Receptor Antagonist ZM241385 Enhances Neuronal Survival after Oxygen-Glucose Deprivation in Rat CA1 Hippocampal Slices. *Br. J. Pharmacol.* **2009**, *157*, 818–830.

(88) Segala, E.; Guo, D.; Cheng, R. K. Y.; Bortolato, A.; Deflorian, F.; Doré, A. S.; Errey, J. C.; Heitman, L. H.; Ijzerman, A. P.; Marshall, F. H.; Cooke, R. M. Controlling the Dissociation of Ligands from the Adenosine A2A Receptor through Modulation of Salt Bridge Strength. *J. Med. Chem.* **2016**, *59*, 6470–6479.

(89) Day, T. J. F.; Honig, B.; Shaw, D. E. A Hierarchical Approach to All-Atom Protein Loop Prediction - Jacobson - 2004 - Proteins: Structure, Function, and Bioinformatics - Wiley Online Library. *Proteins Struct.* **2004**, *55*, 351–367.

(90) Jacobson, M. P.; Friesner, R. A.; Xiang, Z.; Honig, B. On the Role of the Crystal Environment in Determining Protein Side-Chain Conformations. *J. Mol. Biol.* **2002**, *320*, 597–608.

(91) Madhavi Sastry, G.; Adzhigirey, M.; Day, T.; Annabhimoju, R.; Sherman, W. Protein and Ligand Preparation: Parameters, Protocols, and Influence on Virtual Screening Enrichments. *J. Comput. Aided. Mol. Des.* **2013**, *27*, 221–234.

(92) Greenwood, J. R.; Calkins, D.; Sullivan, A. P.; Shelley, J. C. Towards the Comprehensive, Rapid, and Accurate Prediction of the Favorable Tautomeric States of Drug-like Molecules in Aqueous Solution. *J. Comput. Aided. Mol. Des.* **2010**, *24*, 591–604.

(93) Shelley, J. C.; Cholleti, A.; Frye, L. L.; Greenwood, J. R.; Timlin, M. R.; Uchimaya, M. Epik: A Software Program for PKa Prediction and Protonation State Generation for Drug-like Molecules. *J. Comput. Aided. Mol. Des.* **2007**, *21*, 681–691.

(94) Maier, J. A.; Martinez, C.; Kasavajhala, K.; Wickstrom, L.; Hauser, K. E.; Simmerling, C. Ff14SB: Improving the Accuracy of Protein Side Chain and Backbone Parameters from Ff99SB. *J. Chem. Theory Comput.* **2015**.

(95) Zgarbov, M.; Otyepka, M.; Rí Sponer, J.; St Ml, A.; Ban, P.; Cheatham, T. E.; Jure, P. Refinement of the Cornell et Al. Nucleic Acids Force Field Based on Reference Quantum Chemical Calculations of Glycosidic Torsion Profiles. *J. Chem. Theory Comput* **2011**, *7*, 56.

(96) Wang, J.; Wolf, R. M.; Caldwell, J. W.; Kollman, P. A.; Case, D. A. Development and Testing of a General Amber Force Field. *J. Comput. Chem.* **2004**, *25*, 1157–1174.

(97) Bayly, C. I.; Cieplak, P.; Cornell, W. D.; Kollman, P. A. A Well-Behaved Electrostatic Potential Based Method Using Charge Restraints for Deriving Atomic Charges: The RESP Model. *J. Phys. Chem.* **1993**, *97*, 10269–10280.

(98) Wang, J.; Cieplak, P.; Kollman, P. A. How Well Does a Restrained Electrostatic Potential (RESP) Model Perform in Calculating Conformational Energies of Organic and Biological Molecules? *J. Comput. Chem.* **2000**.

(99) Wang, J.; Wang, W.; Kollman, P. A.; Case, D. A. Automatic Atom Type and Bond Type Perception in

Molecular Mechanical Calculations. *J. Mol. Graph. Model.* **2006**, *25*, 247–260.

(100) Frisch G. W.; Schlegel, H. B.; Scuseria, G. E.; Robb, M. A.; Cheeseman, J. R.; Scalmani, G.; Barone, V.; Petersson, G. A.; Nakatsuji, H.; Li, X.; Caricato, M.; Marenich, A. V.; Bloino, J.; Janesko, B. G.; Gomperts, R.; Mennucci, B.; Hratch, D. J., M. J. . T. Gaussian 16, Rev. A.03. *Gaussian, Inc., Wallingford, CT* **2016**.

(101) Case, D. A.; Cheatham, T. E.; Darden, T.; Gohlke, H.; Luo, R.; Merz, K. M.; Onufriev, A.; Simmerling, C.; Wang, B.; Woods, R. J. The Amber Biomolecular Simulation Programs. *J. Comput. Chem.* **2005**, *26*, 1668–1688.

(102) Berendsen, H. J. C.; van der Spoel, D.; van Drunen, R. GROMACS: A Message-Passing Parallel Molecular Dynamics Implementation. *Comput. Phys. Commun.* **1995**, *91*, 43–56.

(103) Darden, T.; York, D.; Pedersen, L. Particle Mesh Ewald: An N·log(N) Method for Ewald Sums in Large Systems. *J. Chem. Phys.* **1993**, *98*, 10089.

(104) Hess, B., Bekker, H., Berendsen, H.J.C. & Fraaije, J. G. E. M. LINCS: A Linear Constraint Solver for Molecular Simulations. Journal of Computational Chemistry. *J. Comput. Chem.* **1997**.

(105) Berendsen, H. J. C.; Postma, J. P. M.; Van Gunsteren, W. F.; Dinola, A.; Haak, J. R. Molecular Dynamics with Coupling to an External Bath. *J. Chem. Phys.* **1984**, No. 18, 1463–1472.

(106) Bussi, G.; Donadio, D.; Parrinello, M. Canonical Sampling through Velocity Rescaling. *J. Chem. Phys.* **2007**, *126*, 014101.

(107) Parrinello, M.; Rahman, A. Polymorphic Transitions in Single Crystals: A New Molecular Dynamics Method. *J. Appl. Phys.* **1981**, *52*, 7182–7190.

(108) Kearsley, S. K. On the Orthogonal Transformation Used for Structural Comparisons. *Acta Crystallogr. Sect. A* **1989**, *45*, 208–210.

(109) Tribello, G. A.; Bonomi, M.; Branduardi, D.; Camilloni, C.; Bussi, G. PLUMED 2: New Feathers for an Old Bird. *Comput. Phys. Commun.* **2014**, *185*, 604–613.

(110) Bonomi, M.; Bussi, G.; Camilloni, C.; Tribello, G. A.; Banáš, P.; Barducci, A.; Bernetti, M.; Bolhuis, P. G.; Bottaro, S.; Branduardi, D.; Capelli, R.; Carloni, P.; Ceriotti, M.; Cesari, A.; Chen, H.; Chen, W.; Colizzi, F.; De, S.; De La Pierre, M.; Donadio, D.; Drobot, V.; Ensing, B.; Ferguson, A. L.; Filizola, M.; Fraser, J. S.; Fu, H.; Gasparotto, P.; Gervasio, F. L.; Giberti, F.; Gil-Ley, A.; Giorgino, T.; Heller, G. T.; Hocky, G. M.; Iannuzzi, M.; Invernizzi, M.; Jelfs, K. E.; Jussupow, A.; Kirilin, E.; Laio, A.; Limongelli, V.; Lindorff-Larsen, K.; Löhr, T.; Marinelli, F.; Martin-Samos, L.; Masetti, M.; Meyer, R.; Michaelides, A.; Molteni, C.; Morishita, T.; Nava, M.; Paissoni, C.; Papaleo, E.; Parrinello, M.; Pfaendtner, J.; Piaggi, P.; Piccini, G. M.; Pietropaolo, A.; Pietrucci, F.; Pipolo, S.; Provasi, D.; Quigley, D.; Raiteri, P.; Raniolo, S.; Rydzewski, J.; Salvalaglio, M.; Sosso, G. C.; Spiwok, V.; Šponer, J.; Swenson, D. W. H.; Tiwary, P.; Valsson, O.; Vendruscolo, M.; Voth, G. A.; White, A. Promoting Transparency and Reproducibility in Enhanced Molecular Simulations. *Nat. Methods* **2019**, *16*, 670–673.

(111) Bonomi, M.; Barducci, A.; Parrinello, M. Reconstructing the Equilibrium Boltzmann Distribution from Well-Tempered Metadynamics. *J. Comput. Chem.* **2009**, *30*, 1615–1621.